Electronic Supplementary Information (ESI)

for

A MOF-derived iron oxide nanorod platform for multiplexed detection of ovarian cancer extracellular vesicle biomarkers

Supplementary Figures

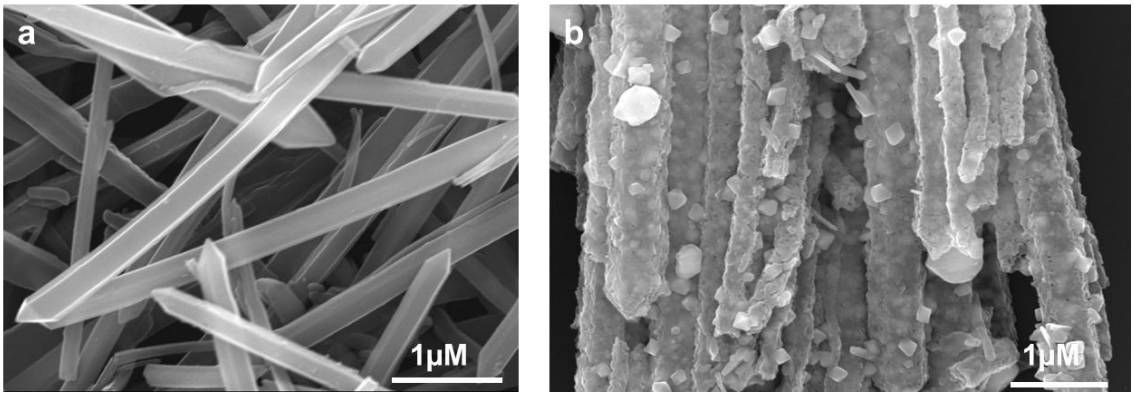

Fig. S1. SEM images of (a) Fe-MOF and (b) MOF-IONRs.

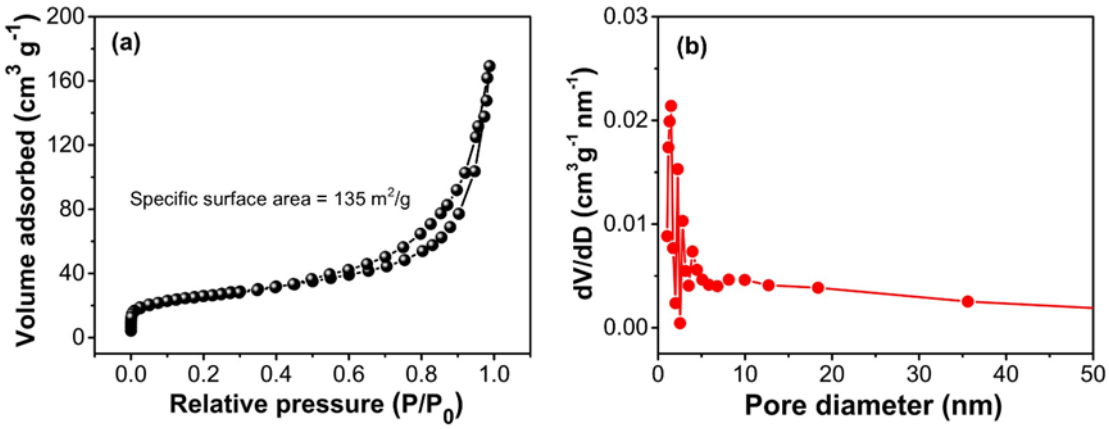

Fig. S2. (a) N_2 adsorption-desorption isotherms and (b) pore size distribution plot of MOF-IONRs.

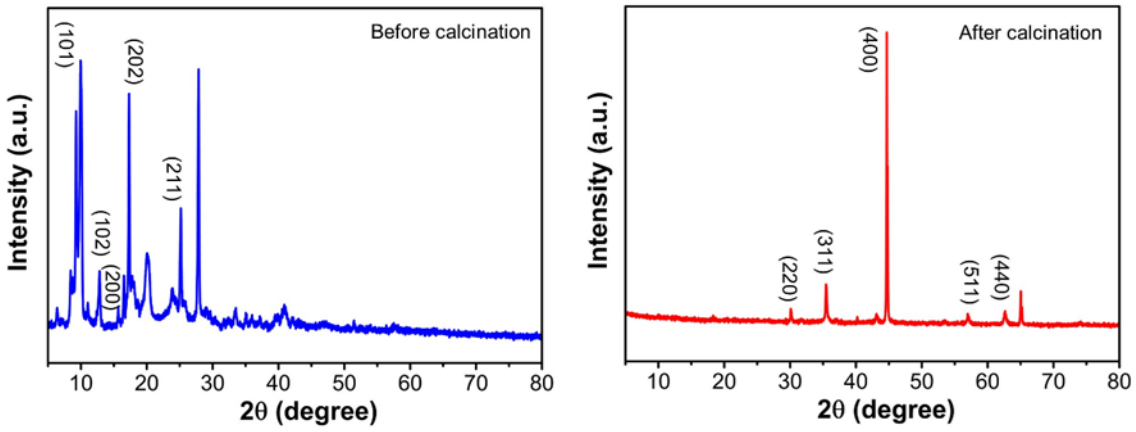

Fig. S3. Wide-angle XRD patterns of Fe-MOF and MOF-IONRs.

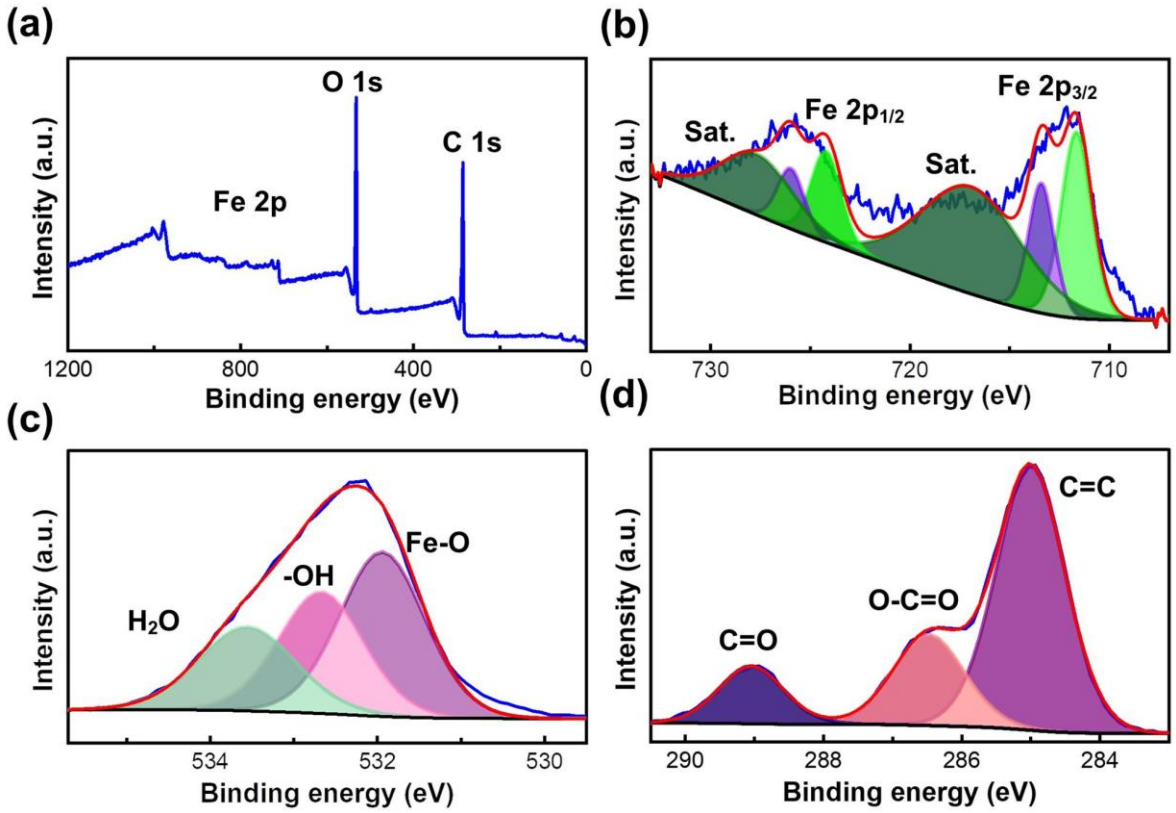

Fig. S4. (a) XPS survey spectrum and high-resolution XPS spectra for (b) Fe 2p, (c) O 1s, (d) C 1s of MOF-IONRs.

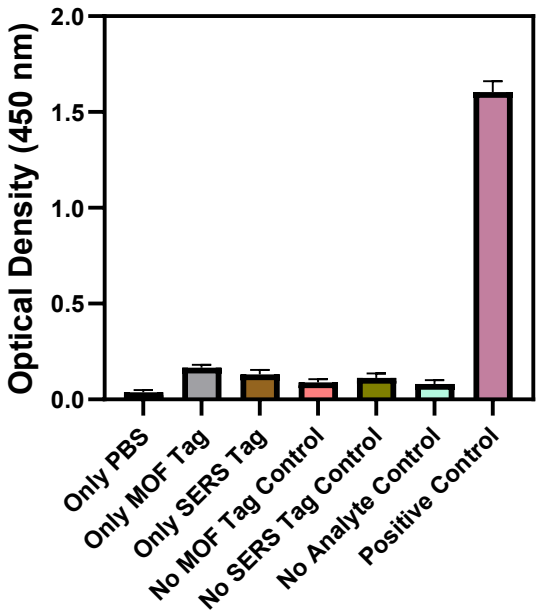

Fig. S5. ELISA absorbance at 450 nm for different control conditions. Bars represent mean optical density (OD) ± SD from replicate (n = 3) wells for each condition: Only PBS, Only MOF tag, Only SERS tag, No MOF tag control (PBS + analyte + SERS Tag conjugated detector antibody), No SERS tag control (MOF-IONRs bound capture antibody + analyte + PBS), No analyte control (MOF-IONRs bound capture antibody + PBS + SERS Tag conjugated detector antibody) , and Positive control (MOF-IONRs bound capture antibody + analyte + SERS Tag conjugated detector antibody). Minimal background signal was observed for all negative or partial controls, whereas the positive control produces a significantly elevated OD.

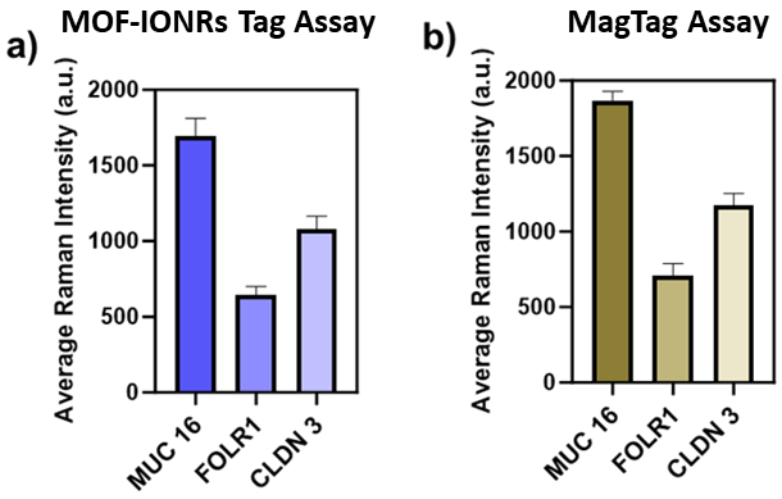

Fig. S6. The average Raman intensities, which indicate the expression levels of the detected biomarkers on isolated EV surfaces, were found to be identical in both the MOF-IONRs Tag and MagTag-facilitated SERS assays.

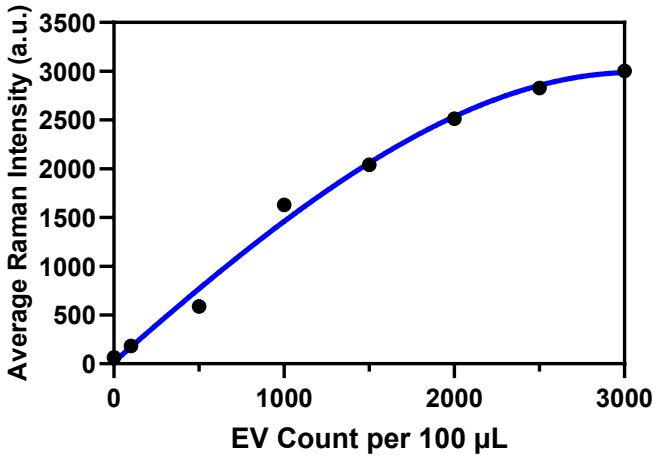

Fig. S7. Polynomial fitting applied to the logarithmic relationship between EV concentration and SERS response, resulting in an R^2 value of 0.9934.

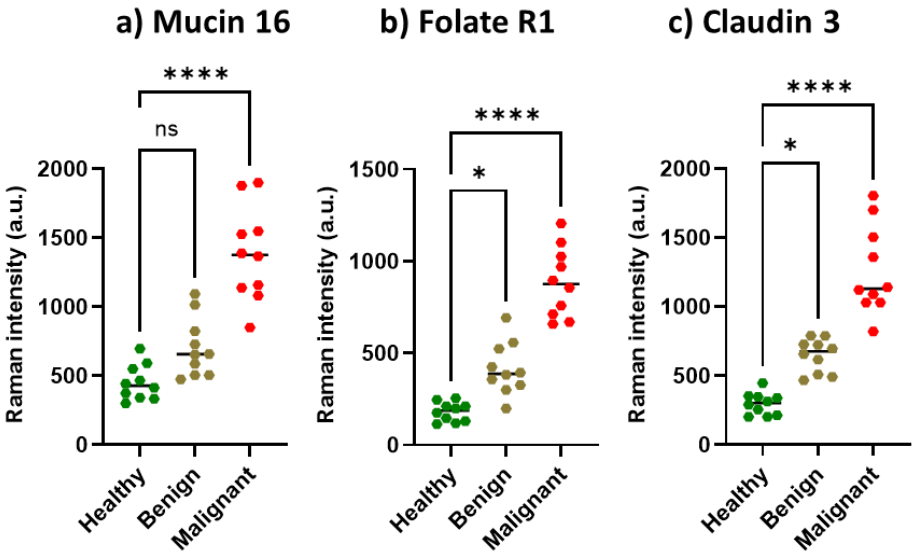

Fig. S8. EV-derived protein biomarkers (MUC16, claudin-3, and FOLR1) in clinical samples from Healthy, Benign, and HGSOC groups (n = 10 per group). Group differences were tested by Kruskal-Wallis with Dunn's post hoc test. Asterisks indicate adjusted significance: **** $p < 0.0001$; ns = not significant.

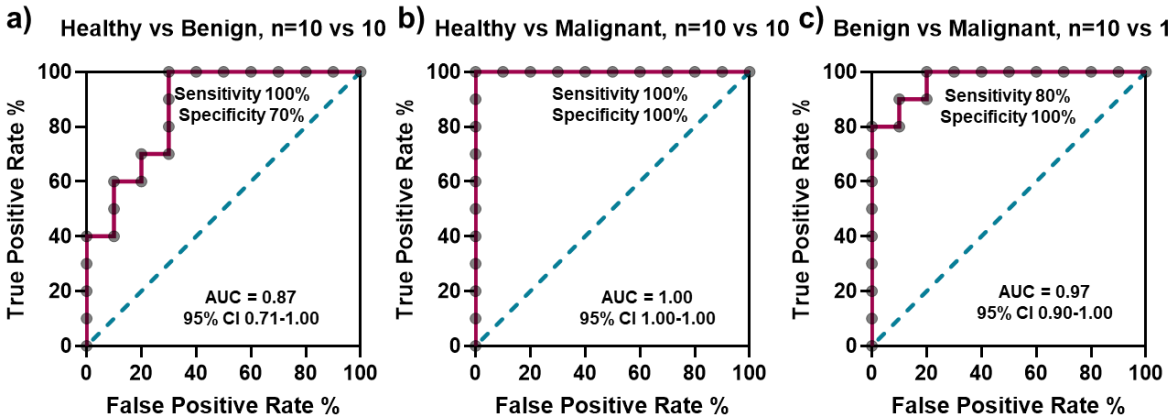

Fig. S9. ROC curves for MUC 16. (a) Healthy vs Benign, (b) Healthy vs Malignant, (c) Benign vs Malignant; n = 10 sample per group. The dot marks the Youden-J operating point with the corresponding sensitivity/specificity shown. AUC (95% CI): (a) 0.87 (0.71-1.00), (b) 1.00 (1.00-1.00), (c) 0.97 (0.90-1.00). The dashed diagonal indicates chance performance (AUC = 0.5). Positive class is the higher MUC 16 group (Benign in a; Malignant in b-c).

Supplementary Tables

Table S1. Comparison of the sensitivity of our SERS-based assay with other reported methods for EV detection

No.	Material	Sensing Method	Detection Limit	Ref.
1	ssDNA attached g-C_3N_4 nanosheets	Colorimetric	13.52×10^5 particles/μL	S1
2.	Fe/Co-MIL-88(NH_2) MOF	Chemiluminescence	1×10^5 particles /mL	S2
3.	Zr-MOF (PCN-224)	Aptasensor	1.0×10^5-1.0×10^7 particles/mL	S3
4	MXene@Ni_3(HITP)$_2$@AuNPs	Electrochemical	13.79 particles/mL	S4
5	PbS QDs	Electrochemical	19 particles/mL	S5
6	SiO_2	Electrochemical	5 particles/uL	S6
7	Fe_3O_4/C	SERS	2.13 particles/μL	This Work

Table S2. Details of patient samples

Characteristic	**Healthy (*n* = 10)**	**Benign (*n* = 10)**	**Ovarian cancer (*n* = 10)**
Age (years)	56 ± 11 (45-72)	62 ± 71 (39-71)	62 ± 12 (39-70)
Pathologic Diagnosis	(-)	(-)	High grade serous 10/10
Clinical stage	(-)	(-)	IIIC (10/10)
Primary or recurrence	(-)	(-)	Primary (10/10)
Optimally debulked	(-)	(-)	10/10

*****_Data are presented as mean ± SD (min-max). (−) Data not applicable._

Table S3. MOF-IONR-based SERS data vs ELISA data for MUC 16 (CA 125) detection

Classifier	Method	AUROC	Sensitivity (95% CI)	Specificity (95% CI)
Healthy vs Benign	Our Platform	0.87	100% (72-100%)	70% (40-89%)
Healthy vs Malignant	Our Platform	1.00	100% (72-100%)	100% (72-100%)
Benign vs Malignant	Our Platform	0.97	80% (49-94%)	100% (72-100%)
Healthy vs Benign	ELISA	0.50	60% (31-83%)	60% (24-76%)
Healthy vs Malignant	ELISA	0.84	80% (49-94%)	100% (72-100%)
Benign vs Malignant	ELISA	0.77	80% (49-94%)	90% (60-98%)

References

S1 S. D. Ibsen, J. Wright, J. M. Lewis, S. Kim, S.-Y. Ko, J. Ong, S. Manouchehri, A. Vyas, J. Akers and C. C. Chen, *ACS Nano*, 2017, **11**, 6641–6651.

S2 Q. Jiang, Y. Xiao, A. N. Hong, Y. Shen, Z. Li, P. Feng and W. Zhong, *ACS Sens.*, 2023, **8**, 1658–1666.

S3 J. Kuang, L. Zhao, S. Ruan, Y. Sun, Z. Wu, H. Zhang, M. Zhang and P. Hu, *Anal. Chim. Acta*, 2024, **1329**, 343234.

S4 W. Cui, L. Qu, Y. Xu, Z. Wang, Y. Gu, S. Tian, F. Qi and H. Pan, *Talanta*, 2025, **282**, 126987.

S5 J. Huang, T. Chen, Y. Zhao, D. Li, Q. Huang, L. Cao, J. Chen, D. Chen, L. Hu and H. Liu, *Chem. Eng. J.*, 2024, **487**, 150616.

S6 D. G. Mathew, P. Beekman, S. G. Lemay, H. Zuilhof, S. Le Gac and W. G. van der Wiel, *Nano Lett.*, 2019, **20**, 820–828.